Spectrochimica Acta Part A: Molecular and Biomolecular Spectroscopy 263 (2021) 120162

Contents lists available at ScienceDirect

Spectrochimica Acta Part A: Molecular and Biomolecular Spectroscopy

journal homepage: www.elsevier.com/locate/saa

Monitorization of polyamide microplastics weathering using attenuated total reflectance and microreflectance infrared spectrometry

Verónica Fernández-González, Jose Manuel Andrade *, Borja Ferreiro, Purificación López-Mahía, Soledad Muniategui-Lorenzo

Group of Applied Analytical Chemistry (QANAP) and Instituto Universitario de Medio Ambiente (IUMA), University of A Coruña, E-15071 A Coruña, Spain

HIGHLIGHTS

- Nylon microplastics identification may be defective if weathering is neglected.
- Usual databases do not contain spectra of environmentally relevant polymers.
- Polyamide weathering was monitored and interpreted chemically.
- A collection of IR indexes reflect overall weathering routes.

GRAPHICAL ABSTRACT

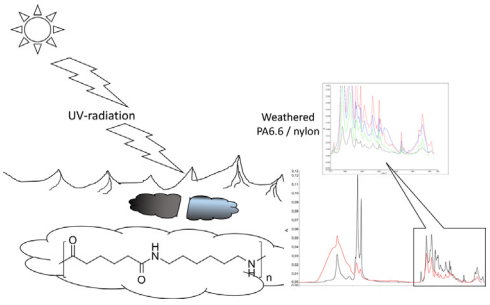

ARTICLE INFO

Article history:
Received 15 January 2021
Received in revised form 2 July 2021
Accepted 4 July 2021
Available online 10 July 2021

Keywords:
Polyamide 6.6
Nylon
Photooxidation
Weathering
Microplastic
Marine environment

ABSTRACT

The EU goal to reduce marine plastic litter by ca. 30% by 2020 stressed the need to deploy analytical methods to ascertain the polymeric nature of a residue. Furthermore, as plastics age under natural conditions and usual databases do not include their weathered spectra, (micro)plastics in environmental samples may be unidentified. In this paper, polyamide (nylon) microplastics weathering was monitored because of its ubiquity in household commodities, clothes, fishery items and industry, whose residues end up frequently in the environment. Infrared spectra (ATR and microreflectance) and Scanning Electron Microscopy (SEM) images were collected periodically while exposing nylon to controlled weathering. It was seen that ATR was more sensitive than microreflectance to monitor the structural evolution of polyamide and that the spectra and the surface of weathered microplastics showed remarkable differences with the pristine material, which stresses the need for considering its evolution when identifying microplastics in environmental studies. The evolution of six band ratios related to the chemical evolution of this polymer are presented. SEM images revealed the formation of secondary microplastics at the most advanced weathering stages of polyamide.

© 2021 The Authors. Published by Elsevier B.V. This is an open access article under the CC BY-NC-ND license (http://creativecommons.org/licenses/by-nc-nd/4.0/).

1. Introduction

The so many advantages that plastics brought to human technology and wellbeing cannot be denied. Unfortunately, their success might also bring about a (so far hidden) planetary boundary threat if we consider the Persson's *et al* studies [1,2]. Their presence in the environment is worldwide recognized, even in very large quantities (think about the oceanic gyres where thousands of plastic items and microplastics accumulate), although it is not still clear the effects they may cause in the different compartments of Nature.

The European Global Strategy on Circular Economy [3,4] targeted actions to reduce plastic consumption, increase its

* Corresponding author.
E-mail address: andrade@udc.es (J.M. Andrade).

https://doi.org/10.1016/j.saa.2021.120162
1386-1425/© 2021 The Authors. Published by Elsevier B.V.
This is an open access article under the CC BY-NC-ND license (http://creativecommons.org/licenses/by-nc-nd/4.0/).

recyclability and reduce its disposal, and it also proposed the development of innovative plastics (e.g., biodegradable). At present, around 50% of plastic residues go to landfill (although this figure varies throughout Europe) and only 25% of the collected plastic is recycled. A major objective of the EU is to reduce plastic marine litter, about 30% by 2020, and, so, the Green paper on plastic waste was deployed [5].

A good example of a plastic commodity is polyamide –PA- (best known commercially as nylon). This is the general term for a broad range of chemical formulations, out of which PA 6 and PA 6.6 outstand for textile and plastic industries. The former gives rise to a commercial product known as Perlon [6] or, more common, Nylon 6 (CAS number 25038–54-4, polycaprolactam) highly similar to PA 6.6 although it absorbs more humidity, and has lower strength and stiffness than that. The latter, PA 6.6 or Nylon 6.6 (CAS number 32131–17-2, poly(hexamethylene adipamide)), is obtained through a condensation polymerization of two monomers each containing 6 carbon atoms –hexamethylenediamide and adipic acid- (from which the name Nylon 6.6 arose). Crystalization is due to strong hydrogen bonding between the chains [7]. The uses and properties of both polymers are almost the same (many times they are mentioned indistinctly) and the choice between the two polymers is often made on non-technical grounds, e.g. local availability, price or familiarity [8].

The worldwide production of PA 6 and PA 6.6 (in the following, PA) raised to 7.8 million tons in 2016 and found many industrial applications [9]. It was reported that 5.7 million tons of polyamide fibers were produced worldwide in 2017, which is about 8% of the worldwide production of synthetic fibers [10]. The most important sales were related to carpet and staple fibers, textiles and industrial filaments (including fishing nets, lines, etc.). Carpets and rugs account for 16% of the PA consumed and are expected to grow at 0.7% per year. North America and Western and Central Europe are the major producers of carpets and rugs, accounting for about 80% of the nylon fiber consumed [11].

The overall consumption of nylon fiber is expected to grow at about 3.5% per year for the next five years, with Northeast Asia accounting for nearly two-thirds of the world's nylon fiber output. PA is also a very relevant engineering plastic for automotive industries (ca. 38% of the PA production), electrical and electronics (21%) [12].

Contrary to other plastics, like PET (whose ubiquitous worldwide presence is obvious due to its use to get disposable containers, like bottles), the PA environmental impact might be not so evident as it tends to sink in seawater and is mostly related to fishing, household and industrial activities, including dry-cleaning, which –most times- end up in wastewater treatment plants [13,14]. As a token of the relevance of PA in the marine environment, some papers can be cited. Thus, the majority of microplastics (MPs) found in a natural protected area at Southern Spain corresponded to PA, likely from a nearby harbour and fishing activities [15]. A river basin polluted by anthropogenic discharges showed PA as the most frequent polymer [16] and it was the second most frequent polymer in fibers collected from fish samples off Northeast Greenland [17] (considering all MPs identified by infrared spectrometry, it was the third most abundant polymer there). PA constituted the second most common type of MPs found in the water column of the Gulf of Lions [18] and two papers discovered also big quantities of PA microparticles in shrimps [19] and in reefs at the South China Sea (second polymer after polypropylene) [20]. Finally, PA was third among the selected MPs that undergone chemical characterization in samples from the Mediterranean area [21], the Baltic sea [22] and the coastal area of Tamil Nadu (India) [23], in the latter case due to recreational and fishing activities.

Despite the number of papers related to the environmental presence of PA in the environment is rising, the evolution of PA microplastics has not been considering in depth and, so, this paper attempts to shed some light on this issue. Not in vain, weathering might be a key factor to study the ad/absorption of pollutants on plastics and their potential impacts in the biota [2].

Infrared spectrometry (IR) has become a *de facto* standard to rigorously identify polymer fragments in the environment. However, as plastics degrade under solar and marine conditions (see, e.g. [2,24,25]). Their IR spectra have to be compared to a collection of known degraded polymer spectra to find out the best match. Unfortunately, to best of the authors' knowledge, almost no commercial database contains series of degraded polymers and, so, many plastic fragments may be misidentified in environmental samples. This topic was discussed in recent papers [25,26,27,28]. Notwithstanding, it is critical to keep in mind that this problem is insidious because even if the evolution of a plastic is known the variety of commercial brands (including different compositions and additives) and the complex natural conditions might modify the weathering routes/products for that plastic (see, e.g. [28] for a good discussion on this topic).

The major objectives of this paper are twofold: first, to use ATR –attenuated total reflection- and reflectance IR microspectrometry to monitor PA 6.6 weathering (the latter being applied first time for this purpose). Second, to relate the changes observed into the spectra to polymeric structural modifications. As this polymer is not studied frequently in the microplastics literature it is expected that this work will help both scientists focused on studying the evolution of MP in the sea (for whom some band ratios are proposed) and those performing routine measurements aimed at identifying and quantifying microplastics in environmental samples (for whom the evolution of the spectral characteristics are vital).

2. Materials and methods

2.1. Samples

The PA 6.6 polymer used in this study corresponds to the commercial name 'Ultramid', from BASF, whose density was 1.13 g. cm^{-3}; melting temperature 260 °C. Two presentations were available: pellets, ca. 4 mm diameter, and powder, with a size Gaussian distribution centred around 100 μm (standard deviation ca. 80 μm). The polyamide was fabricated so as to contain as few additives as possible, and it was included in a collection of microplastics developed for the JPI-Oceans-funded project BASEMAN.

A device for the standardized simulated weathering of powdered and pelletized PA microplastics was used. In brief, it resembles the natural seawater conditions by setting continuous agitation, sand erosion, sunlight irradiation and oxidative conditions. It uses two metal halide lamps whose emission spectra matches that of the solar radiation at the Earth surface (medium latitude). The overall UV/VIS illuminance was 12,200 lx in a continuous mode (i.e., no day-light cycles). The total irradiation time was eleven weeks (ca. 1850 irradiation hours). More details can be found elsewhere [29].

For the seawater weathering conditions 10 g of PA powder and 20 g of PA pellets were placed in 1000 mL Pyrex cylinders, along with siliceous sea-sand and natural, filtered (10 μm) seawater. For the dry conditions (emulating solar irradiation at the shoreline) the same quantities were placed in 12 cm diameter Petri dishes. Control samples were also considered (pellets and powder submerged in seawater at dark). The contents of the dishes were stirred manually each two or three days. Seawater, dry and control aliquots were taken each fortnight (15, 30, 45, 60 and 75 days; corresponding to 360, 720, 1080, 1440 and 1800 irradiation hours, respectively).

2.2. Apparatus and equipments

A Spectrum 400 FTIR spectrometer, Perkin Elmer, equipped with a horizontal one-bounce single-reflection ATR (attenuated total reflection) diamond (MIRacle, Pike), operating in the 4000–600 cm^{-1} mid-IR region, 30 scans/sample, apodization Beer-Norton strong, 4 cm^{-1} nominal resolution, was employed throughout. All ATR spectra were corrected for light-reflectance penetration and baseline displacement.

A Perkin Elmer Spotlight 200i IR microscope was used to perform the reflectance measurements. Each item (pellet or granule) was measured twice (changing its position) and the resulting spectra were averaged. The experimental setup was: nominal resolution: 4 cm^{-1}; number of scans: 200; spectral range: 3500–600 cm^{-1}; nominal aperture: 100 μm (adjusted whenever the scanned part of the grain required it); apodization: Beer-Norton, strong; spectral processing: Kubelka-Munk transformation (for pellets) and normalization 10% plus Kramers-Kronig (for powders). All spectra were baseline corrected using multipoint baseline correction. Note that the surface characteristics of the item under measurement affect data processing due to their possible main interaction with the IR beam: pellets allow for measuring almost flat surfaces, making the reflection almost specular, whereas for powders the irregular shape of the grain's surface makes reflection more diffuse.

Reflectance measurements were selected instead of transmittance ones because the former are the most common ones in literature. Also, reflectance spectra are independent of the thickness of the particles (transmittance can be affected by the effective pathlength) and can be applied straightforwardly. Further, as reflectance is a surface-characterization technique it can detect polymer ageing quite accurately (a superficial phenomenon). Note also that the size of the particles handled in this work (>70 μm) is far from the physical limitations that can occur when very small (<20 μm) particles are measured. This allows reflectance to be applied safely to most common environmental monitoring studies (for instance, when Neustonic or manta-trawl nets are used their pore sizes are usually around 200–330 μm).

A JEOL JSM-6400 Scanning Electron Microscope (SEM), coupled to an Energy-dispersive X-ray spectroscopic microanalysis device (EDXA, Oxford INCA Energy 200) was employed. All samples were covered with a gold film using a cathodic spraying system (BALTEC SCD 004) prior to the SEM measurements.

3. Results and discussion

3.1. Chemical interpretation of the IR spectra

In this section, PA spectra are interpreted in detail and related to the chemical processes PA undergoes during weathering. This is in order here as most previous reports focused only on partial aspects of the spectrum and a full interpretation was not found. Thus, a brief review is presented. With respect to PA degradation, although the cleavage of N-C bonds at short radiations (254 nm) to yield amines and aldehydes was clearly studied, it is not evident what happens within the solar spectral region (300 nm and higher) [30]. Four principal weathering routes for PA are described, of which the first two (see next paragraphs) are the major ones, however notice that all them may occur almost conjunctly:

(i) Photooxidation can be initiated by chromophoric impurities from fabrication (unbounded or partially bounded functional groups). They lead to an initiation step that can involve either the photolysis of hydroperoxides or ketones formed during fabrication (which is a common mechanism for most polyolefins –Norrish I and II mechanisms-) [31].
(ii) Photooxidation can also be due to oxygen-induced reactions because of charge transfer complexes [30,32]. This seems particularly feasible for PA6.6 and involves direct photolysis of the amide bond [32].
(iii) The hydrolytic degradation route is attributed to the especial susceptibility of the amide bond to acid- and basic-catalysed hydrolysis [30]. The catalysing metals might be those present naturally in seawater and those used at the production catalysts or embedded salts [33].
(iv) Finally, thermal oxidation –a non photooxidative process- is also possible by means of the abstraction of hydrogen atoms on the methylene groups close to the nitrogen atom of the amide group [34].

Roughly, photodegradation would lead to aldehydic and acidic groups, whereas hydrolysis would lead to carboxylic acid and amine groups [30]. In essence, the mechanisms of thermal and photochemical oxidation are identical, but for their onset [31]. Although thermal oxidation should not be a major weathering route in this study, because neither the water nor the air temperatures surpassed 30 °C, it cannot be disregarded totally (as it will be shown later on).

The ATR spectra of pristine (*as received*) pellets and powder and last aliquots of weathered PA under the three weathering setups (seawater plus irradiation; dry plus irradiation and control-dark) are shown in Fig. 1. First, it is observed that no new distinctive spectral bands appear throughout weathering, as reported for outdoor weathering of ropes [30]. However, this might be a consequence of the broad spectral bands and their mutual overlaps.

All PA spectra show the typical CH–related spectral bands (stretching, at 2863 and 2934 cm^{-1}; and bending, 1450 and 1375 cm^{-1}). The amide group yields three major sets of characteristic bands [7,35,36,37]:

1. The NH stretch-free motion at ca. 3400 cm^{-1}; the NH stretch H-bonded, around 3300 cm^{-1}; and a NH bending overtone around 3070 cm^{-1} (which might coincide with a weak NH stretch H-bonded band [35,36] and C-N stretching [38]). Here, the most distinguishable band is the peak at 3300 cm^{-1}, which increases roughly with ageing, likely because of two main processes: i) the photolysis of the amide bond to yield amines [33,34], and ii) the introduction/appearance of hydroxyl groups in the polymer. This band is much broader for seawater-submerged microplastics than for dry weathering, where a relatively sharp peak (associated to free N-H stretching, ca. 3400 cm^{-1}) is more alike that reported by Ksouri *et al.* [35].
   The hydroxyl groups (broad band between 3000-3500 cm^{-1}) would correspond, mostly, to water absorbed in the plastic (despite secondary or tertiary alcohols or even hydrogen bonds between carboxylic groups cannot be disregarded). In effect, it was reported that PA 6.6 absorbs more than 8% of its weight in 100% relative humidity at room temperature [35]. The hygroscopic introduction of the OH groups in the structure is due to the presence of the polar functional groups and it occurs, mainly, into the amorphous regions of the polymer [35]. Note that in our case the two experimental setups that involved immersion in seawater yielded spectral profiles different from the dry weathering setup (see Fig. 1).
2. A strong sharp band around 1633 cm^{-1} corresponding to the carbonyl (C = O) stretching (it is also called Amide I band). Its overall increase (see Fig. 1) characterizes the final products of both the photodegradation and hydrolysis reactions because

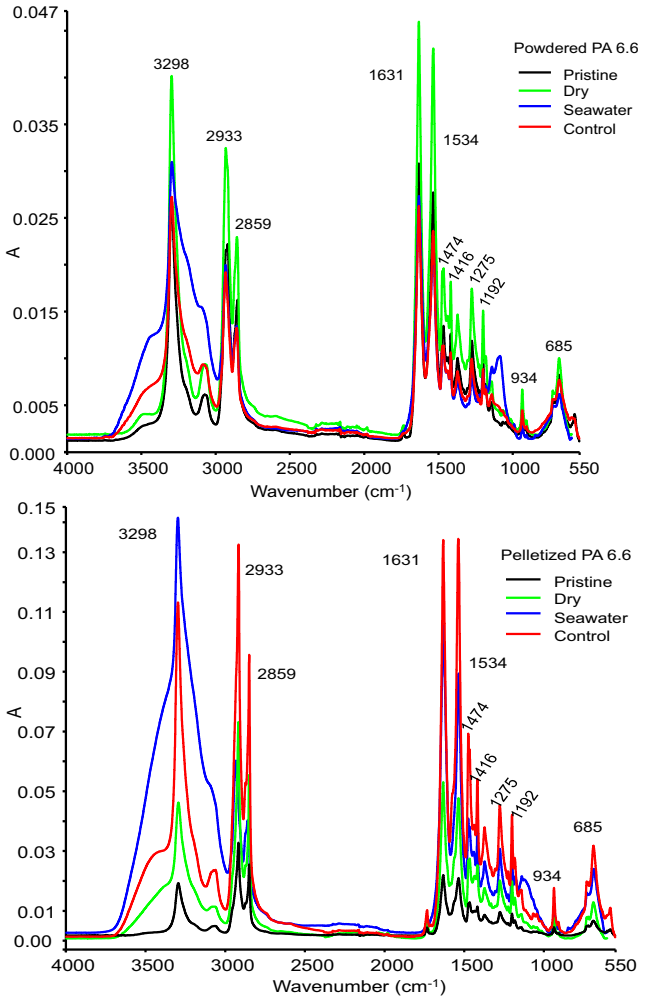

Fig. 1. Comparison of the PA spectra for powder and pellets obtained by ATR: pristine (*as received*), and last aliquots of controls, dry weathering and seawater weathering.

aldehydes, ketones and acid groups display highly close strong absorption bands in this region. Therefore, any assignation to a particular functional group is troublesome.

3. The band at 1537 cm^{-1} (Amide II band) is associated to the NH mono-substituted amide bending plus the C-N stretching. Another band could appear around 1650 cm^{-1}, although overlapped with the Amide I band [35,36]. The Amide II band rises clearly with ageing (as well as the 696 cm^{-1} one, related to end NH_2 groups [39]) and, hence, indicates the polymer chain scission. Observe (Fig. 1) that the bands are more intense for the PA samples weathered under dry conditions, likely suggesting a participation of thermal degradation processes (contrary to the PA seawater-immersed ones).

Some other interesting bands can be considered:

i. The unique band in the spectrum that decreased clearly with ageing was at 1735 cm^{-1}, with two interpretations:

a. The presence of cyclopentanone derivatives originated at fabrication process, whose content decreases during thermo-oxidation processes [40]. Noteworthy, this peak is only seen for pellets weathered under dry conditions, which might support the reported steady dissapearance of the residual cyclopentanone. That peak is neither present in powdered samples nor in seawater submerged ones and, so, we hypothetized that cyclopentanone disappeared there much faster thanks to the much smaller size of the solid grains (in seawater it would leach to the water).

b. Another possibility is to relate this band to a vibration form of hydrogen-bonded carbonyl groups. PA has charged regions in the polymer chain becoming attracted to each other, which causes the individual polymer chains to fold back over on itself and for other polymer chains to similarly be attracted to each other [41]. As this occurs mostly in the amorphous regions, the increase on crystallinity (to be discussed later) would lead to the disappearance of this band.

ii. The band centred at 1150 cm^{-1} (not visible in the reflectance spectra) is very prominent for the seawater conditions and it could suggest tertiary or secondary alcohols, ketones (asymmetric C-C-C stretching, with central C containing the O), ethers (symmetric and asymmetric stretching of C-O-C), esters (C-O-R bending) and/or the typical combination band of the carboxylic acids (C-O stretching plus OH bending). All these structures are compatible with reported end products for photooxidation and/or thermo-oxidation of PA [31,32,34,38].

iii. Two weak bands appear around 930 and 920 cm^{-1}, related to the CO-NH in-plane vibration [42], and another one at 696 cm^{-1}, related to end NH_2 groups [39].

iv. A relevant property of any polymer is crystallinity, which was studied extensively by Li and Goddard [43] and Vasanthan and Salem [42]. They established that out of four possible forms only two are stable; α and γ [43]. The γ form (amorphous) tends to convert into the former (crystalline), even when only mechanical stress is applied at room temperature. In the α form the plane of the amide group and that of the $(CH_2)_5$ group are parallel, while in the γ form they are approximately perpendicular. H-bonds are formed between the two forms. Vasanthan and Salem established [7,42] that the bands at 936 and 1200 cm^{-1} are due to the crystalline conformation. They correspond to the CO – NH in-plane vibration [7] (alternately, to the C-CO amide axial stretching [44]) and the symmetrical CH_2 twist-wag angular deformation out of plane [7], respectively). A shoulder at 924 cm^{-1} (CO – NH in-plane stretching) and 1136 cm^{-1} (C – C stretching) correspond to the amorphous structure [7]. The bands at 936 and 1200 cm^{-1} are usually sharper than the other two. The crystalline fraction can be calculated from the IR spectrum as $8.8 \cdot (A_{936}/A_{1630})$ because the C = O band at 1630 cm^{-1} does not depend on crystallinity [7]. Other possible bands to characterize crystallinity are those at 976, 1030, and 1074 cm^{-1} [39] but they are used less. Unfortunately, these bands are very weak in the reflectance spectra so these calculations become compromised.

With regards to the reflectance spectra of pellets although those characteristics hold on (Figure 2), some interesting differences can be underlined:

i. Broad bands due to the –OH groups are not seen, which simplifies the identification of several peaks (mostly, the NH stretch-free motion at ca. 3400 cm^{-1}; the NH stretch H-bonded, around 3300 cm^{-1}; and a NH bending overtone

around 3070 cm^{-1}). However, it is worth noting that the band ca. 3400 cm^{-1} was not clearly visible until the most weathered stages of the polymer.

ii. Spectra are dominated by strong and quite narrow peaks which, in essence, correspond to the amide functional groups. On the contrary, other bands related to -e.g.- the CH and OH moieties of the polymeric skeleton yield weak bands. Thus, despite the reflectance spectra of the pellets appear less noisy than their ATR counterparts (Fig. 2), they are less sensitive and, unfortunately, this will have consequences in some band ratios, as it will be shown in next sections.

The microreflectance spectra of the small granules (70–300 μm) were much less intense than the ATR ones and also than those for pellets measured by microreflectance (Fig. 2). This is attributed to the diffuse scattering and radiation interactions caused by the rough and irregular surface of the granules. This adds to the intrinsic reduced intensity of the microreflectance technique. The most intense and clear bands are associated to the typical amide group, whereas the other bands are less clear. This hampers both the chemical interpretation and the calculations related to the less intense bands. Therefore, they will not be considered in more detail in next sections. Nevertheless, it is derived immediately from these facts that the use of adequate (in this case, home-made) databases is of absolute, paramount importance to identify polymers from field samples. In effect, current spectral databases will not be of use for microreflectance spectra as they are based on transmittance or absorbance units.

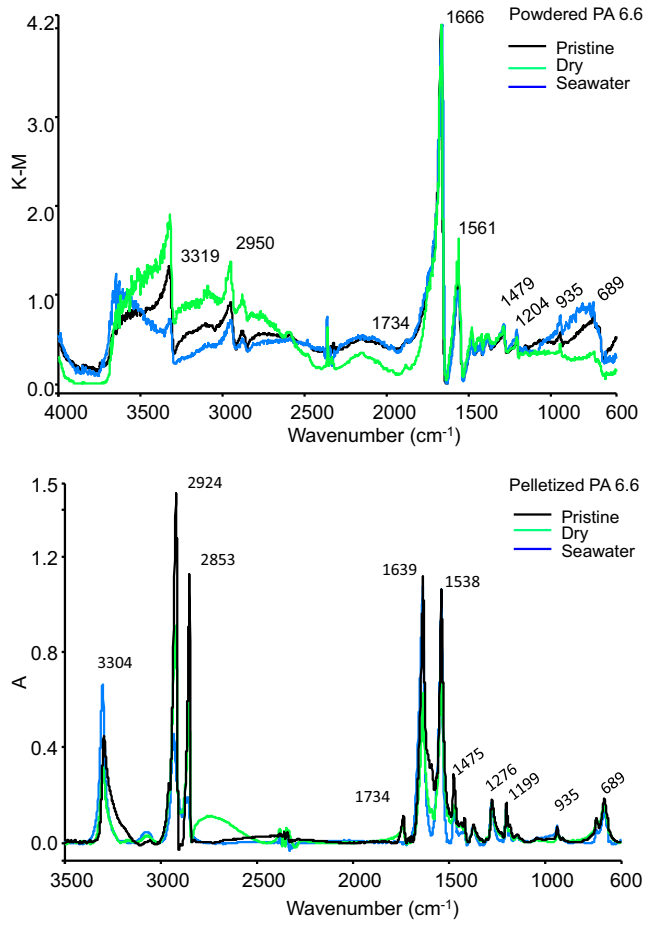

Fig. 2. Comparison of the PA spectra for powder (Kubelka-Munk ordinate units) and pellets obtained by reflectance microspectrometry: pristine (*as received*), and last aliquots of controls, dry weathering and seawater weathering.

3.2. Monitoring PA6.6 evolution using spectral indexes

It is common practice in weathering studies to monitor the evolution of the polymer using band ratios. They normalize bands associated to functional groups of interest against a reference peak that ideally is unaffected by the evolution of that functional group and remains constant with time. Here, the C-H bending peak located around 2915 cm^{-1} was selected. To the best of our knowledge weathering ratios have not still been established for PA 6.6 and, hence, several options are evaluated here, including some employed to monitor other polymers [45,46]. Another approach to monitor weathering may be to consider spectral differences between the spectra of the aged aliquots and that of the pristine polymer, as a referee suggested. This option was not explored in the present manuscript but we acknowledge its feasibility. To simplify readability, hereinafter comments and studies will be given for the ATR spectra. Particular details will be added for the reflectance spectra whenever appropriate (in general, as a comparison with the ATR results).

3.2.1. The carbonyl index

Defined as the A_{1640}/A_{2914} integrated areas ratio, the carbonyl index considers the C=O stretching band and has been of widespread use when studying different polymers [28,45,46]. The only similar application for PA is a work from Gijsman *et al.* [32], although they used a subtraction, not really a ratio.

In Fig. 3**a** the evolution of the index is shown for both pellets and powder. It raises with time for all weathering setups, being higher for the simulated marine conditions (either because of the kinetics being faster into seawater or because of the displacement of the chemical equilibria due to the release of the products to the aqueous phase). A steady, smooth increment is seen even for the control samples (pellets or powder kept at dark, immersed in seawater), which confirms that the mere presence of water interpenetrates the bonds between the –NH and C=O groups and degrade the polymer [35,41]. No doubt, this process is much slower when light is absent, but it occurs. Indeed, note that the samples weathered without water led to a lower carbonyl formation than the controls.

Although the general rising trend is clear, three stages can be seen in the plots, and they agree with previous studies [39,40]. A first, fast increase indicates the oxidative degradation (mainly in the amorphous phase, where oxygen can diffuse fast. Then, a plateau is observed probably because the oxidative process slows down due to a reduction in the amount of amorphous phase; finally, a continuous increase because of the degradation of the crystalline phase [40]. For powdered microplastics, the dry and control conditions lead to almost coincident situations and despite an initial weathering the trends are very smooth. This agrees with Goodridge *et al.* [41] and they attributed the evolution to a time-dependent change of the amorphous phase and reported that this is a general phenomenon for all polymeric materials.

Finally, a comparison of the spectra in Fig. 3**a** reveals that weathering seems more pronounced for the pellets, likely because the plastic powder might had undergone already some previous degradation and, so, their initial states are not exactly the same. This seems reinforced by the carbonyl ratio for the 'pristine' (*as received*) samples, 1.08 for powder and 0.52 for pellets. Recall that powder fabrication implies a huge stress on the polymer and this has been shown to increase the physical and chemical degradation [34]. The final sudden increment for the dry powder after the eighth week can only be explained by a 'collapse' (i.e., strong degradation) of the polymer. This hypothesis was confirmed by

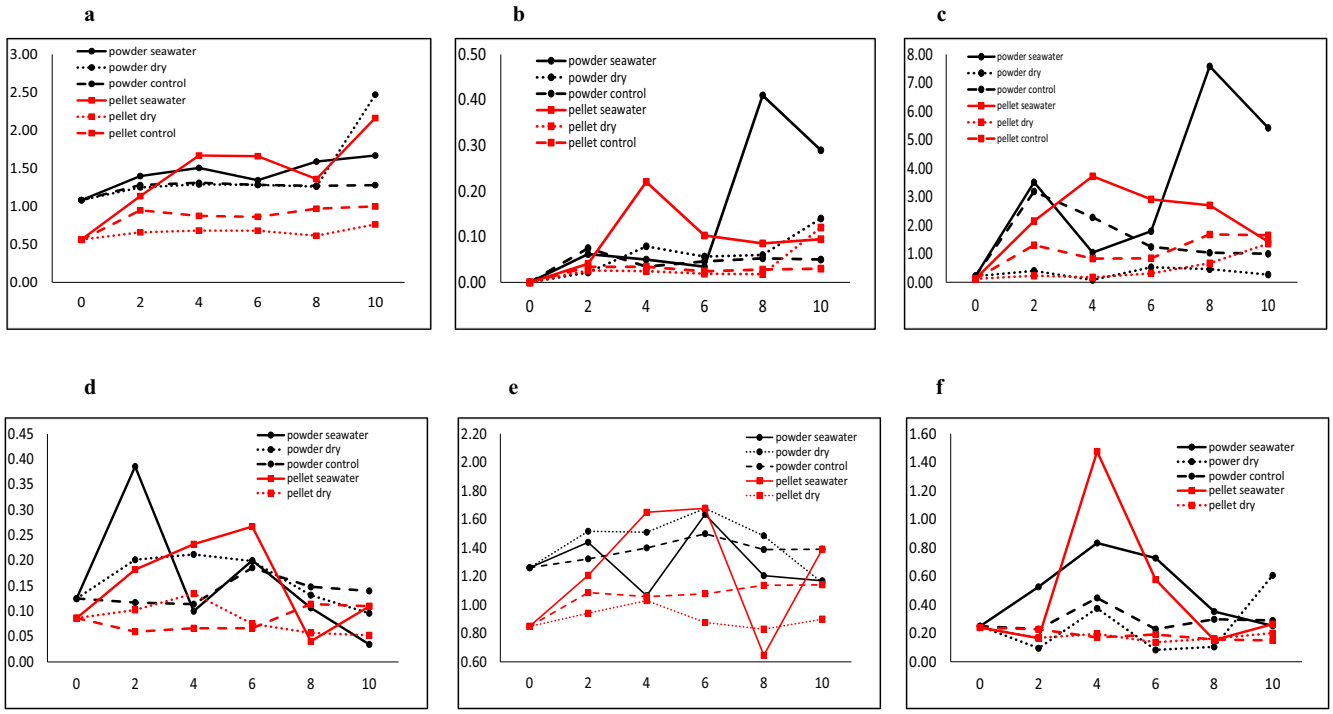

Fig. 3. Evolution of several functional indexes to monitor PA weathering using ATR: a) C=O; b) C-O; c) O-H; d) crystallinity; e) amide II; and f) long chains. The x-axis represents the number of weathering weeks (0 = means 'pristine' –as received- polymer).

scanning electron microscopy (see **Figure SM1f** in the supplementary material and explanations at the corresponding section below).

Calculations of this index for the reflectance spectra of pellets allowed to derive analogous conclusions (Fig. 4**a**).

3.2.2. The C-O index

This index, defined as the ratio of the $A_{1000\text{-}1200}/A_{2914}$ integrated bands, is intended to characterize carboxylic acids and/or esters. Unfortunately, for PA 6.6 the region between 1000 and 1200 cm^{-1} includes several peaks from different functional groups (see discussions above), which makes it unspecific for this bond. Note that for the reflectance spectra this is not the case but the peaks seen there became weak or very weak. The overall behaviour of the index parallels the C=O one (Fig. 3**b**). Powdered PA in seawater showed a remarkable increment after the sixth weathering week (which is not seen so dramatically for the C=O group). The reflectance-derived index for pellets showed the same general behaviour (Fig. 4**b**), although without the remarkable increase after the 6th week that was seen for the ATR spectra. The overall evolution profile for the C-O index is also very similar to the OH index, discussed below.

3.2.3. The O-H index

The evolution of the O-H index (A_{3300}/A_{2914} integrated bands ratio) represents changes in the intermolecular interactions among carboxylic groups and the introduction of OH groups in the polymer. However, the ATR broad band at ca. 3300 cm^{-1} is not specific for the O-H group as the sharp band in its centre corresponds to the NH vibration and H-bonds between the C=O and NH groups of different chains when water is absent [44]. In our case, we do have aqueous/humid conditions and, so, from a practical point of view for current environmental studies, we decided to consider the overall area as a 'proxy' for the overall OH groups.

As for the C=O index, three major stages can be seen for the OH evolution during PA weathering (Fig. 3**c**). Despite the reflectance bands ca. 3300 cm^{-1} were narrower than the ATR ones, the index had essentially the same behaviour (but for a slight increase in the reflectance index at the 8th week for pellets in seawater, which is not seen for ATR data), Fig. 4**c**. A first rise attributed to the initial degradation of the polymer, followed by a plateau and a slight final increment. This latter stage is not seen for the pellets submerged into seawater using ATR although it is clear in the reflectance spectra (Fig. 4**c**). After the sixth week, the ATR indicates that the degradation of the powdered PA in seawater is much higher than for any other assay. This may be explained because the powder had large floating times in the water surface despite the probes were agitated continuously by an air stream. Every day the powder in the surface was sent back manually to the water. The pellets, on the contrary, were at the surface marginally. Submerged pellets and powder became more degraded than their dry counterparts.

3.2.4. The crystallinity index

The index was defined as the A_{936}/A_{1640} ratio [42], although in order to use a unique reference peak, the alternative A_{936}/A_{2914} ratio is proposed in this work (it was verified that both calculations yielded the same graphical pattern). Fig. 3**d** shows the evolution of this index during weathering. The overall profile agrees very well with previous discussions for the other indexes. Crystallinity has not a uniform evolution throughout weathering. Some authors reported on its diminution with weathering, likely due to a severe chain scission after prolonged exposure of PA [31,39,40]. On the contrary, Arrieta et al. [30] informed about crystallinity increments. This discrepancy may be explained by a first increase on crystallinity due to rearrangements of the molecular fragments caused by photooxidation in the amorphous region; then a stabilization and finally a decrease, because even the crystalline phase is degraded and cleavages chains from the crystal surface [31,39,40]. This effect would be more relevant with prolonged ageing as the entanglement network reduces and only Van der Waals interactions maintain the polymer in the final stages [35]. This

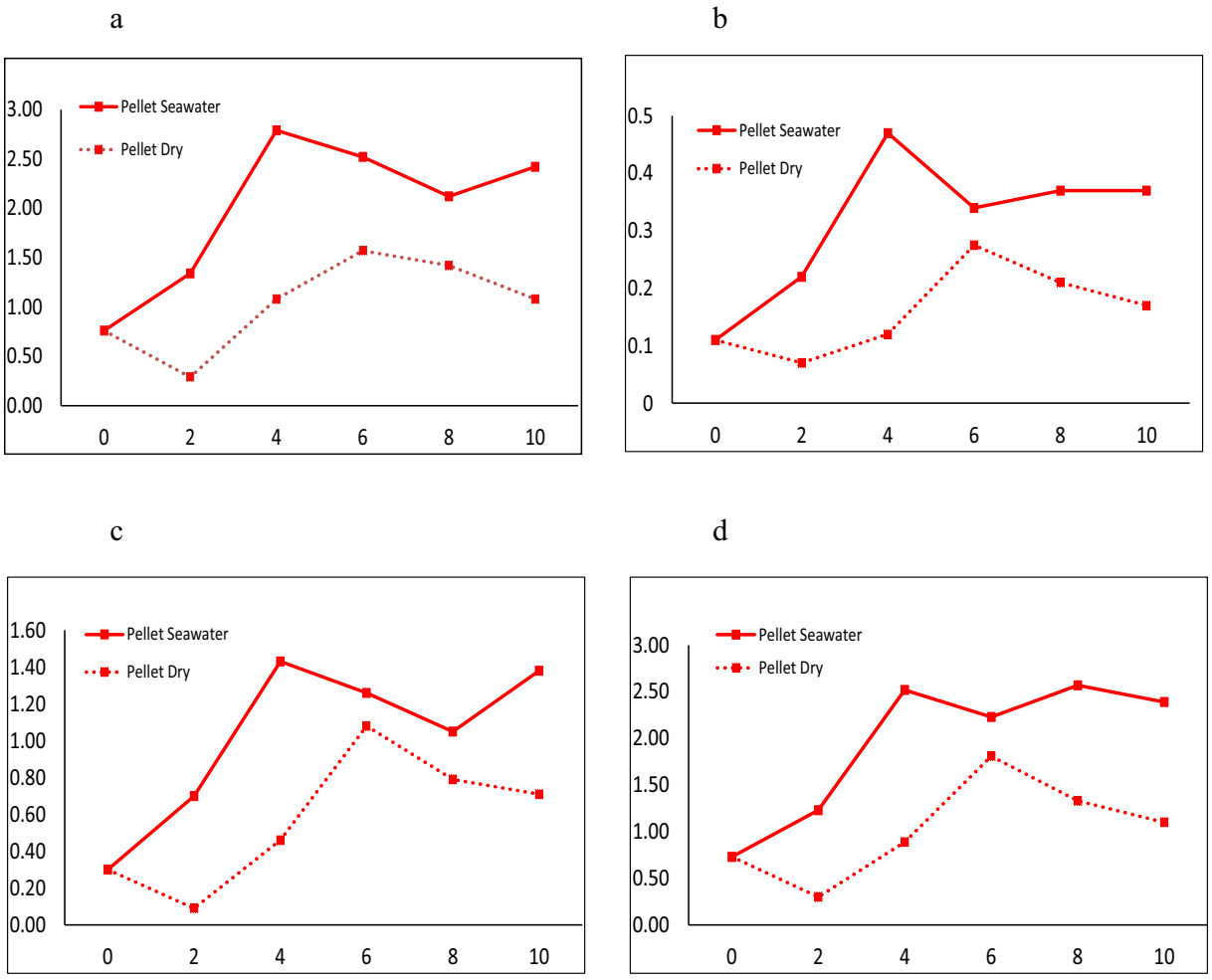

Fig. 4. Evolution of several functional indexes to monitor PA weathering using reflectance spectrometry: a) C = O; b) C-O; c) O-H; d) amide II. The x-axis represents the number of weathering weeks (0 = means 'pristine' –as received- polymer).

complex sequence in crystallinity is seen also in our experimental results:

It increases quite sharply during the first fortnight (which corresponds to a rearrangement of the scissored chains/fragments in the amorphous regions), then it reaches a plateau (but for the powder in seawater) and, finally, decreases clearly after the sixth week (ca. 1000 h of irradiation). The relevant drop in PA crystallinity for powder in seawater around four weeks can be attributed (as for the OH index) to its flotation (which means it received more irradiation than submerged pellets), combined with a release of molecular fragments from the degraded polymer to the aqueous phase. Then, a second rearrangement of the amorphous phase seems to occur (an increase on the crystallinity index) which finally gets degraded as well. Note that although both control samples remain quite stable their crystallinity increased slightly at the end, likely due to a reorganization of the amorphous phase after some hydrolysis/thermal processes.

When the reflectance spectra for pellets were considered, the index showed only a smooth, steady increasing pattern, likely because the bands involved in this index were weak and, so, scarcely sensitive to the minor variations. In particular, the drop after the 6th week was not seen, only a plateau was observed instead (figure not shown here).

3.2.5. The amide II index

This index had not been defined previously in the literature, and is proposed as the A_{1537}/A_{2914} ratio. Despite the initial ratios for pellets and powder are different (Fig. 3**e)** their behaviours are similar and resemble the crystallinity index. The powdered samples show the three major steps explained for the indexes above (ATR spectra). The pellets submerged in seawater present two clear stages, considering both ATR and microreflectance (a steady increase until the sixth week, after which a degradation occurs, leading to a new reorganization after the eighth week, Fig. 4**d**). The pellets under dry irradiation had the same pattern as the submerged ones although less intense.

3.2.6. The Branched- and long-chains indexes

Finally, two indexes are of potential interest here. They evaluate how the amount of branched and long hydrocarbon chains evolve [47,48,49,50]. The ***branched-chain index*** is calculated as the $A_{1376}/A_{1450+1376}$ ratio whereas the long-chains index is the $A_{724}/A_{1450+1376}$ ratio. The former has not been too informative in this study because it showed a relative random pattern, maybe because the band at 1376 cm^{-1} is not only associated to the symmetric bending of the CH bond (in CH_3 groups) and the asymmetric bending of CH (in CH_2 units), but to other groups like the CN stretching plus the in-plane NH deformation [44].

On the contrary, the ***long chain index*** (which, in essence, measures the number of linearly bonded CH_2 groups) was more informative. All assays show (Fig. 3**f**) a decrease on the length of the CH_2 chain during the first two weeks (but for the powdered PA submerged into the seawater, which shows a steady increase). This opposes to the increment in the C=O, C-O and O-H indexes (initial

oxidative degradation in the amorphous phase, [39,40]) and it confirms that the total amount of longer fragments of the polymer (-$(CH_2)_n$-) decreases (and, so, that oxidation occurs throughout chain scission, as Arrieta *et al* [30] suggested). At the fourth week a sudden and sharp increase of the long chain index points towards the recrystalization process (which coincides with the decrease on the C=O, C-O and O-H indexes). Finally, after the eighth week, the long chain index stabilizes and it does not recover the previous values, probably because the oxidation proceeds faster. The powder weathered under dry conditions have a slightly different behaviour and after the eighth week it increases again, coinciding with the slight decrease in the C-O and O-H indexes, pointing towards a second recrystallization. These two indexes were not very informative when reflectance spectra was considered, likely because the bands involved are very weak.

3.3. Scanning electron microscopy and energy-dispersive X-ray analyses

SEM (scanning electron microscopy) studies were also done in order to characterize further the weathering processes. First, the weathering for pellets will be discussed.

Original pellets *as received* showed the typical fibrils associated to the ductile fracture occurring at the cutting stage of the polymer [31]. Some exfoliation linked to the fracture planes and a relevant void (supposedly a gas bubble) were observed (**Figure SM1, a and b, supplementary material**).

After 10 weeks of simulated sea conditions, the surface revealed clearly eroded, with a porous appearance in some parts of the pellet, cracks, scratches, wells and, of course, salt deposits (**Figure SM1, c and d**). The latter are of importance here because we visualized many sites where the surface was clearly eroded and highly affected by the presence of salt crystals. The Energy-dispersive X-ray analyses, EDXA, showed that they were mostly NaCl or $CaCl_2$. Indeed the surface was clearly carved and the crystals grown at those voids (see zoomed view in **Figure SM1c**).

Scratches and cracks can be explained by thermal stress and mechanical impacts but also by the internal stress caused by the water molecules entering the structure and causing hydrolysis and swelling [35]. Carving could be explained partly by the fact that some metals were reported to accelerate PA degradation (e.g., Co and Ni) [33,40]. Although those studies were done with metals included in the polymer formulations, they are indeed present in seawater and their pro-oxidation effect should not be disregarded [31]; more specific studies would be needed to clarify this.

With respect to the dry weathering setup, PA pellets showed also clear grooves, flakes (see zoomed view in **Figure SM1e**) and small scratches. However, the most dramatic visualization was a region where the polymer was totally fragmented following parallel planes (**Figure SM1f**), similar to those seen in **Figure SM1e**. Recall that PA is mostly constituted by a lamellar structure [43]. Despite it might appear a collection of salt deposits, the EXDA elemental analysis indicated that their elemental composition was dominated by C; in addition, their shape do not match the cubic appearance of salt crystals. Hence, it was concluded that it was degraded PA.

When it comes to the *as received* powdered PA the typical fibrils and fracture planes can be seen (**Figure SM2a and SM2b, supplementary material**); as well as sharp angles and well defined borders. After the 10-weeks seawater weathering the borders appeared fragmented, rounded and without the original fibrils, denoting clear erosion patterns. The fragmentation planes were blurred by erosion and many grooves. In some pictures (not shown here) small cracks and wells appeared. Noteworthy, those voids were quite often associated to included salt crystals. Their elemental composition revealed Cl, Mg, K, Ca and O; whose most probable matches are salts of the corresponding chlorides and MgO.

A number of small fragments was also seen in most degraded granules, some of them still unreleased from their main body (**Figure SM2c)**. This would evidence the well-known reported formation of secondary microplastics from larger pieces. [2]. In addition, clear crazing and ploughing were seem in some granules (**Figure SM2d**).

With regard to the dry conditions, the mechanical erosion and degradation of the borders of the granules were much less relevant (as expected). However, more flakes could be observed in turn, along with crazing and voids (**Figure SM2e)** even in a stratified way (**Figure SM2f)** where some very small particles can be observed, likely due to superficial mechanical and thermal stress. The humid conditions of the room due to water evaporation from the adjacent probes containing seawater might facilitate water absorption which stresses the structure of the polymer [35].

4. Conclusions

The ageing of polyamide 6.6 was monitored under simulated natural weathering conditions. With regards to the qualitative identification of particles in environmental samples, it was found that the evolution of PA does not depend on its form (pellets or powder) nor on the experimental setup (seawater-submerged or dry conditions), but for some more pronounced evolution when the dried setup was considered, mostly for powder. A remarkable finding was that the evolution of the spectral bands do not follow a steady pattern. Instead, the spectral indexes denote cyclic evolutions, as explained in literature. The IR spectral profiles of the original and weathered PA microplastics were different and this stresses the importance of considering this evolution whenever microplastics from the environment are characterized. The simplest option is to include weathered spectra of PA in the databases driving the searches. This is of most importance whenever reflectance spectra are measured.

About the evolution of the polymer, ATR and microreflectance spectra put forward the two major photooxidative weathering pathways for PA. They show in general three stages. First, a fast increase indicates the oxidative degradation (mainly in the amorphous phase, where oxygen can diffuse fast); then a plateau probably due to a slow down on the oxidative process in the amorphous phase; finally, a continuous increase because even the crystalline phase gets degraded. It was seen that reflectance microspectrometry had less complex spectra although they were less sensitive than ATR, and this caused that only the monitoring indexes calculated from the most intense bands had the same general behaviour.

The overall large increase of the so-called Amide I band characterizes the final products of the photodegradation and hydrolysis reactions. The Amide II band rises clearly with ageing (as well as the 696 cm^{-1} one, related to terminal NH_2 groups) and, hence, characterizes the polymer chain scission. The outstanding general increase of the broad band centred ca. 3300 cm^{-1} points towards the introduction/appearance of hydroxyl groups in the polymer. They would correspond mostly to water absorbed in the plastic, mainly into the amorphous regions of the polymer.

The carbonyl index raises for all weathering setups with time, being higher for the simulated marine conditions. The same happens for the C-O index and, less obvious, the O-H one. The crystallinity index reinforces those conclusions as it increases quite sharply during the first fortnight (rearrangement of the scissored chains/fragments in the amorphous regions), then it reaches a plateau (but for the powder in seawater) and, finally, decreases clearly after the sixth week.

Regarding the SEM measurements, the surface of the most weathered pellets and powder grains revealed clearly eroded, with a porous appearance in some parts, cracks, scratches, wells and salt deposits. The surface was clearly carved and many crystals were seen at those voids, which might suggest that superficial salts may potentiate mechanical particle degradation. The most eroded grains revealed the formation of secondary microplastics.

CRediT authorship contribution statement

Verónica Fernández-González: Conceptualization, Methodology, Formal analysis. **Jose Manuel Andrade:** Conceptualization, Methodology, Software, Validation, Formal analysis. **Borja Ferreiro:** Methodology, Software, Validation, Formal analysis. **Purificación López-Mahía:** Conceptualization, Validation. **Soledad Muniategui-Lorenzo:** Conceptualization, Validation.

Declaration of Competing Interest

The authors declare that they have no known competing financial interests or personal relationships that could have appeared to influence the work reported in this paper.

Acknowledgements

This work was supported through the JPI-Oceans BASEMAN and MicroplastiX projects, sponsored by the Spanish Ministry of Science and Innovation (Agencia Estatal de Investigación) - partially financed by the European Regional Development Fund program- (Grants: PCIN-2015-170-C02-01; PCIN- PCI2020-112145 and CTM2016-77945-C3-3-R, ARPA-ACUA). The Program 'Consolidación e Estructuración de Unidades de Investigación Competitiva' of the Galician Government (Xunta de Galicia) is also acknowledged (Grant: ED431C-2017/28)

Appendix A. Supplementary material

Supplementary data to this article can be found online at https://doi.org/10.1016/j.saa.2021.120162.

References

[1] L.M. Persson, M. Breitholtz, I.T. Cousins, C.A. de Wit, M. MacLeod, M.S. McLachlan, Confronting unknown planetary boundary threats from chemical pollution, Environ. Sci. Technol. 47 (22) (2013) 12619–12622, https://doi.org/10.1021/es402501c.
[2] A. Jahnke, H.P.H. Arp, B.I. Escher, B. Gewert, E. Gorokhova, D. Kühnel, M. Ogonowski, A. Potthoff, C. Rummel, M. Schmitt-Jansen, E. Toorman, M. MacLeod, Reducing Uncertainty and Confronting Ignorance about the Possible Impacts of Weathering Plastic in the Marine Environment, Environ. Sci. Tech. Lett. 4 (2017) 85–90, https://doi.org/10.1021/acs.estlett.7b00008.
[3] Communication from the commission to the European Parliament, the Council, the European Economic and Social Committee and the Committee of the Regions. Closing the loop - an EU action plan for the circular economy. COM (2015) 614
[4] Communication from the Commission to the European Parliament, the Council, the European Economic and Social Committee and the Committee of the Regions. A European Strategy for Plastics in a Circular Economy. COM (2018) 28
[5] Green Paper on a European Strategy on Plastic Waste in the Environment. COM (2013) 123.
[6] www.textileschool.com/ 467/polyamide-fibres-manmade-artificial-fibres/; last access August 1, 2018.
[7] N. Vasanthan, Cristalinity determination of Nylon 66 by density measurement and Fourier Transform infrared (FTIR) spectroscopy, J. Chem. Educ. 89 (2012) 387–390, https://doi.org/10.1021/ed200398m.
[8] https://www.azom.com/article.aspx?ArticleID=442, last access November 15, 2020.
[9] https://www.plasticsinsight.com/resin-intelligence/resin-prices/polyamide/, last access November 15, 2020.
[10] https://www.statista.com/statistics/649908/polyamide-fiber-production-worldwide/, last access November 15, 2020.
[11] https://ihsmarkit.com/products/nylon-fibers-chemical-economics-handbook.html, last access November 15, 2020.
[12] M. Scheibitz, R. Kaneko, P. Spies, Polyamide 6 and 66 (PA6 and PA66), Kunststoffe International 10 (2016) 40–44.
[13] E.A. Gies, J.L. LeNoble, M. Nöel, A. Etemadifar, F. Bishay, E.R. Hall, P.S. Ross, Retention of microplastics in a major secondary wastewater treatment plant in Vancouver, Canada. Mar. Poll. Bull. 133 (2018) 553–561, https://doi.org/10.1016/j.marpolbul.2018.06.006.
[14] I.E. Napper, R.C. Thompson, Release of synthetic microplastic plastic fibres from domestic washing machines: effects of fabric type and washing conditions, Mar. Pollut. Bull. 112 (2016) 39–45, https://doi.org/10.1016/j.marpolbul.2016.09.025.
[15] V.M. León, I. García-Agüera, V. Moltó, V. Fernández-González, L. Llorca-Pérez, José M. Andrade, S. Muniategui-Lorenzo, J.A. Campillo. PAHs, pesticides, personal care products and plastic additives in plastic debris from Spanish Mediterranean beaches. Science of the Total Environment 670 (2019), pp 672–684. Doi: 10.1016/j.scitotenv.2019.03.216
[16] M. Yan, H. Nie, K. Xu, Y. He, Y. Hu, Y. Huang, J. Wang, Microplastic abundance, distribution and composition in the Pearl River along Guangzhou city and Pearl River estuary, China. Chemosphere 217 (2019) 879–886, https://doi.org/10.1016/j.chemosphere.2018.11.093.
[17] S. Morgana, L. Ghigliotti, N. Estévez-Calvar, R. Stifanese, A. Wieckzorek, T. Doyle, J.S. Christiansen, M. Faimali, F. Garaventa, Microplastics in the Arctic: A case study with sub-surface water and fish samples off Northeast Greenland, Environmental Pollution 242 (2018) 1078–1086, https://doi.org/10.1016/j.envpol.2018.08.001.
[18] C. Lefebvre, C. Saraux, O. Heitz, A. Nowaczyk, D. Bonnet, Microplastics FTIR characterisation and distribution in the water column and digestive tracts of small pelagic fish in the Gulf of Lions, Mar. Poll. Bull. 142 (2019) 510–519, https://doi.org/10.1016/j.marpolbul.2019.03.025.
[19] M.S. Hossain, M.S. Rahman, M.N. Uddin, S.M. Sharifuzzaman, S.R. Chowdhury, S. Sarker, M.S.N. Chowdhury, Microplastic contamination in Penaeid shrimp from the Northern Bay of Bengal, Chemosphere 238 (2020), https://doi.org/10.1016/j.chemosphere.2019.124688 124688.
[20] Y. Huang, M. Yan, K. Xu, H. Nie, H. Gong, J. Wang, Distribution characteristics of microplastics in Zhubi Reef from South China Sea, Environ. Poll. 255 (2019), https://doi.org/10.1016/j.envpol.2019.113133 113133.
[21] A.V. Filgueiras, J. Gago, J.A. Campillo, V.M. León, Microplastic distribution in surface sediments along the Spanish Mediterranean continental shelf, Environ. Sci. Poll. Res. 26 (21) (2019) 21264–21273, https://doi.org/10.1007/s11356-019-05341-5.
[22] M.B. Zobkov, E.E. Esiukova, A.Y. Zyubin, I.G. Samusev, Microplastic content variation in water column: The observations employing a novel sampling tool in stratified Baltic Sea, Mar. Poll. Bull. 138 (2019) 193–205, https://doi.org/10.1016/j.marpolbul.2018.11.047.
[23] N. Sathish, K.I. Jeyasanta, J. Patterson, Abundance, characteristics and surface degradation features of microplastics in beach sediments of five coastal areas in Tamil Nadu, India. Mar. Poll. Bull. 142 (2019) 112–118, https://doi.org/10.1016/j.marpolbul.2019.03.037.
[24] A.L. Andrady, Microplastics in the marine environment, Mar. Poll. Bull. 62 (2011) 1596–1603, https://doi.org/10.1016/j.marpolbul.2011.05.030.
[25] A.B. Silva, A.S. Bastos, C.I.L. Justino, J.P. da Costa, A.C. Duarte, T.A.P. Rocha-Santos, Microplastics in the environment: challenges in analytical chemistry, a review, Anal. Chim. Acta. 1017 (2018) 1–19, https://doi.org/10.1016/j.aca.2018.02.043.
[26] A. Karami, A. Golieskardi, Y.B. Ho, V. Larat, B. Salamatinia, Microplastics in eviscerated flesh and excised organs of dried fish, Sci. Rep. 7 (2017) 5473, https://doi.org/10.1038/s41598-017-05828-6 (9 pages).
[27] P. Ribeiro-Claro, M.M. Nolasco, C. Araújo, Chapter 5-characterization of microplastics by Raman spectroscopy, in Comprehensive Analytical Chemistry Handbook. Vol 75 (Characterization and analysis of microplastics). Elsevier. 2017
[28] A. ter-Halle, L. Ladirat, M. Martignac, A.F. Mingotaud, O. Boyron, E. Perez, To what extent are microplastics from the open ocean weathered?, Environ Poll. 227 (2017) 167–174, https://doi.org/10.1016/j.envpol.2017.04.051.
[29] J. Andrade, V. Fernández-González, P. López-Mahía, S. Muniategui, A low-cost system to simulate environmental microplastic weathering, Mar. Poll. Bull. 149 (2019), https://doi.org/10.1016/j.marpolbul.2019.110663 110663.
[30] C. Arrieta, Y. Dong, A. Lan, T. Vu-Khanh, Outdoor weathering of polyamide and polyester ropes used in fall arrest equipment, J. Appl. Polym. Sci. 130 (5) (2013) 3058–3064, https://doi.org/10.1002/app.39524.
[31] P. Cerruti, M. Lavorgna, C. Carfagna, L. Nicolais, Comparison of photo-oxidative degradation of polyamide 6,6 films stabilized with HALS and CuCl2+KI mixtures, Polym. 46 (2005) 4571–4583, https://doi.org/10.1016/j.polymer.2005.03.065.
[32] P. Gijsman, G. Meijers, G. Vitarelli, Comparison of the UV-degradation chemistry of polypropylene, polyethylene, polyamide 6 and polybutylene terephthalate, Polym. Degrad. Stabil. 65 (1999) 433–441, https://doi.org/10.1016/S0141-3910(99)00033-6.
[33] E. Dümichen, U. Braun, R. Kraemer, P. Degelmann, R. Senz, Thermal extraction combined with thermal desorption: a powerful tool to investigate the thermos-oxidative degradation of polyamide 66 materials, J. Anal. Appl. Pyrol. 115 (2015) 288–298, https://doi.org/10.1016/j.jaap.2015.08.006.
[34] X. Zhao, X. Li, L. Ye, G. Li, Stress-accelerated photothermal oxidative aging behaviour of polyamide 6, J. Thermoplast. Compos. 27 (11) (2014) 1573–1586, https://doi.org/10.1177/0892705713495437.

[35] I. Ksouri, O. De Almeida, N. Haddar, Long term ageing of polyamide 6 and polyamide 6 reinforced with 30 % of glass fibers: physicochemical, mechanical and morphological characterization, J. Polym. Res. 24 (8) (2017) 133–145, https://doi.org/10.1007/s10965-017-1292-6.
[36] J. Morcillo, R. Madroñero. Aplicaciones prácticas de la espectroscopia infrarroja. Edited by Universidad de Madrid, Madrid, 1962.
[37] R.T. Conley, Espectroscopia infrarroja, Edit. Alhambra, Madrid, 1979.
[38] C. El-Mazry, M.B. Hassine, O. Correc, X. Colin, Thermal oxidation kinetics of additive free polyamide 6–6, Polym. Degrad. Stabil. 98 (2013) 22–36, https://doi.org/10.1016/j.polymdegradstab.2012.11.002.
[39] A. Bienik, B. Lipp-Symonowicz, S. Sztajnowski, Influence of the structure of polyamide 6 fibers on their agein under intensive insolation conditions, Polimery 54 (11–12) (2009) 840–844, https://doi.org/10.14314/polimery.2009.840.
[40] P. Cerruti, C. Carfagna, Thermal-oxidative degradation of polyamide 6,6 containing metal salts, Polym. Degrad. Stabil. 95 (2010) 2405–2412, https://doi.org/10.1016/j.polymdegradstab.2010.08.014.
[41] R.D. Goodridge, R.J.M. Hague, C.J. Tuck, Effect of long-term ageing on the tensile properties of a polyamide 12 laser sintering material, Polym. Test. 29 (2010) 483–493, https://doi.org/10.1016/j.polymertesting.2010.02.009.
[42] N. Vasanthan, D.R. Salem, Infrared spectroscopic characterization of oriented polyamide 66: band assignment andand crystallinity measurement, J. Polym. Sci. (Part B) 38 (2000) 516–524, https://doi.org/10.1002/(SICI)1099-0488(20000215)38:4<516::AID-POLB3>3.0.CO;2-Y.
[43] Y. Li, W.A. Goddard III, Nylon 6 Crystal Structures, Folds, and Lamellae from Theory, Macromolecules 35 (2002) 8440–8455, https://doi.org/10.1021/ma020815n.
[44] N.K. Pramanik, M.S. Alam, R.K. Khandal, Electron beam irradiation of Nylon 66: characterization by IR spectroscopy and viscosity studies, Int. J. Innovat. Res. Sci Engineer. Tech. 4 (1) (2015) 18547–18555, https://doi.org/10.15680/IJIRSET.2015.0401019.
[45] K. Rajakumar, V. Sarasvathy, A. Thamarai Chelvan, R. Chitra, C.T. Vijayakumar, Natural Weathering Studies of Polypropylene, J. Polym. Environ. 17 (2009) 191–202, https://doi.org/10.1007/s10924-009-0138-7.
[46] J. Brandon, M. Goldstein, M.D. Ohman, Long-term aging and degradation of microplastic particles: Comparing in situ oceanic and experimental weathering patterns, Mar. Poll. Bull. 110 (2016) 299–308, https://doi.org/10.1016/j.marpolbul.2016.06.048.
[47] O. Abbas, N. Dupuy, C. Rebufa, L. Vrielynck, J. Kister, A. Permanyer, Prediction of source rock origin by chemometric analysis of Fourier Transform infrared-attenuated total reflectance spectra of oil petroleum: evaluation of aliphatic and aromatic fractions by self-modeling mixture analysis, Appl. Spectrosc. 60 (3) (2006) 304–314, https://doi.org/10.1366/000370206776342508.
[48] A. Permanyer, L. Douifi, A. Lahcini, J. Lamontagne, J. Kister, FTIR and SUVF spectroscopy applied to reservoir compartmentalization: a comparative study with gas chromatography fingerprints results, Fuel 81 (2002) 861–866, https://doi.org/10.1016/S0016-2361(01)00211-3.
[49] P. Fresco Rivera, R. Fernández Varela, M.P. Gómez Carracedo, F. Ramírez Villalobos, D. Prada, S. Muniategui, J.M. Andrade, Development of a fast analytical tool to identify oil spillages employing infrared spectral indexes and pattern recognition techniques, Talanta 74 (2007) 163–175, https://doi.org/10.1016/j.talanta.2007.05.047.
[50] J.M. Andrade, P. Fresco, S. Muniategui, D. Prada, Comparison of oil spillages using mid-IR indexes and 3-way Procrustes rotation, matrix-augmented principal components analysis and parallel factor analysis, Talanta 77 (2008) 863–869, https://doi.org/10.1016/j.talanta.2008.07.044.